

# Accelerated Self-Healing Via Ternary Interpenetrating Microvascular Networks

Christopher J. Hansen, Scott R. White, Nancy R. Sottos, and Jennifer A. Lewis\*

Self-healing materials with dual interpenetrating microvascular networks enable two-part healing chemistries and repeated healing of damage in a localized region.<sup>[1]</sup> However, due to slow healing kinetics, multiple days are required between damage events to recover mechanical performance under ambient conditions. By directly writing a third interdigitated microvascular network within these epoxy coating/substrate architectures to enable *in situ* thermal regulation, the characteristic healing time is reduced by an order of magnitude. Specifically, this third network provides a conduit for circulating a temperature-controlled fluid that rapidly heats the locally damaged region leading to a sharp reduction in the time required for mechanical property restoration.

## 1. Introduction

Biological systems employ microvasculature networks to accomplish a range of critical functions, including tissue regeneration, thermal regulation, and nutrient transport. Biomimicry of these diverse functions in synthetic materials is achieved by embedding a network of interconnected microchannels. Several emerging applications have recently been demonstrated, including self-healing materials,<sup>[1,2]</sup> active cooling networks,<sup>[3,4]</sup> and tissue cultures.<sup>[5]</sup> For example, self-healing materials benefit from the introduction of microvascular networks that allow both repetitive healing and the use of new healing chemistries.<sup>[1,6,7]</sup> An early approach to self-healing materials relied on damage-induced rupture of microcapsules filled with dicyclopentadiene (DCPD) monomer that interacts with Grubbs' catalyst embedded in the matrix, but only exhibited a single-event healing.<sup>[8–10]</sup> The first microvascular-based system, pioneered by Toohy et al.,<sup>[6]</sup> revealed that a single damage region

could be healed repeatedly using the same chemistry. In their approach, an epoxy coating/substrate architecture was constructed, which contained a single microvascular network that mimics human skin. The microvascular transport of DCPD fluid to a crack opened within the coating allows for repeated healing of a single damage region up to seven cycles before localized catalyst depletion.

The introduction of multiple interpenetrating microvascular networks within these self-healing constructs overcomes the above limitations by supplying both healing components as fluids.<sup>[7]</sup> Hansen et al. demonstrated that a dual micro-

vascular network design enables the use of inexpensive epoxy-based healing chemistries to achieve autonomous healing of up to at least 30 repeated cycles.<sup>[1]</sup> By embedding isolated microvascular networks in close proximity to one another, two-part liquid healing systems are sequestered within the substrate and react only after damage induces their release to the crack plane. To date, dual microvascular networks have been integrated in multiple structural geometries, including substrates with brittle coatings,<sup>[1,7]</sup> bulk structural polymers,<sup>[11]</sup> and sandwich composite structures.<sup>[12,13]</sup> From the broad range of suitable healing chemistries, epoxy resin and amine hardener systems are typically chosen due to their low cost and wide availability in bulk quantities. However, these systems exhibit slow reaction rates, diffusion, and mixing within the crack plane. Ambient microvascular healing requires substantial time intervals ( $\geq 48$  h) to recover a significant fraction of their original mechanical strength.<sup>[1,7,11,13]</sup>

Acceleration of mechanical recovery requires an increase in the epoxy reaction kinetics to quicken the rebonding of the fracture plane. Reaction kinetics for monomeric and oligomeric epoxides in the presence of amines are characterized by an Arrhenius temperature dependence.<sup>[14]</sup> As such, small temperature increases can produce significant acceleration of the epoxy cure rate. The ability to thermally accelerate mechanical restoration has recently been demonstrated in the microcapsule-based healing system<sup>[15]</sup> through the incorporation and resistive heating of shape-memory alloy wires across the fracture interface. However, this approach is not readily compatible with current microvascular fabrication techniques.

Successful implementation of thermally accelerated healing depends critically upon the integration of a localized heating capability. Many engineering structures that would benefit from accelerated healing are large-scale, including wind turbine blades or aircraft wings, which preclude bulk thermal annealing.

C. J. Hansen, Prof. S. R. White, Prof. N. R. Sottos, Prof. J. A. Lewis  
Autonomic Materials Systems Group  
Beckman Institute for Advanced Science and Technology  
University of Illinois at Urbana-Champaign  
Urbana, IL 61801, USA  
E-mail: jalewis@illinois.edu

C. J. Hansen, Prof. N. R. Sottos, Prof. J. A. Lewis  
Department of Materials Science and Engineering  
University of Illinois at Urbana-Champaign  
Urbana, IL 61801, USA

Prof. S. R. White  
Department of Aerospace Engineering  
University of Illinois at Urbana-Champaign  
Urbana, IL 61801, USA

DOI: 10.1002/adfm.201101553

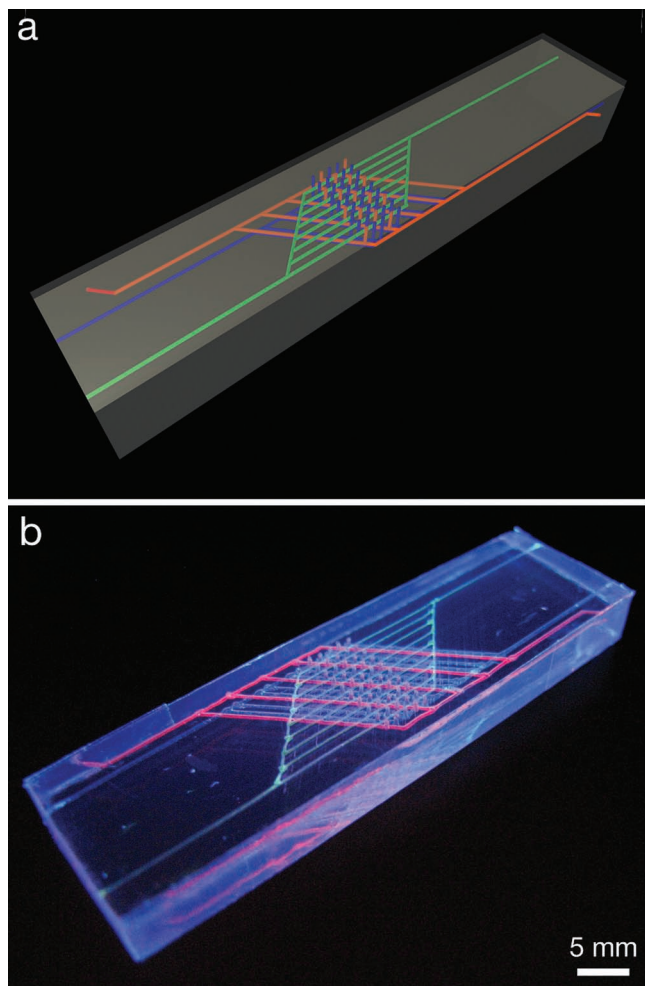


**Figure 1.** (a) Schematic view of epoxy coating/substrate architecture with embedded interpenetrating microvascular networks. Two of these networks house epoxy resin (blue) and hardener (red), while the third network provides thermal control (green) to accelerate healing kinetics after damage occurs. (b) Corresponding optical image of this novel self-healing system fabricated by direct-write assembly and then imaged with different fluorescent dye solutions within each network.

Moreover, these structures often contain integrated components, such as microelectronics, that cannot tolerate excessive thermal loads. Hence, targeted, localized heating offers an efficient approach to accelerate healing of the damage region *in situ*, while leaving a majority of the surrounding structure undisturbed.

Here, we report the assembly and characterization of self-healing materials with embedded ternary interpenetrating microvascular networks in an epoxy coating/substrate architecture (Figure 1a). The networks are fabricated by direct-write assembly of two fugitive inks, in which one ink defines the three microvascular networks and the other ink functions solely as a spacer to isolate each network. Two of the microvascular networks are devoted to supplying the epoxy resin and hardener healing agents, while the third network circulates a thermally regulated fluid. We first characterize the bulk curing kinetics of this epoxy system over the temperature range of interest. Next, we investigate the effect of thermally accelerated healing on mechanical restoration

of these coating/substrate architectures. Finally, we evaluate the extent of healing agent mixing in the crack plane as well as the integrity of network flow using fluorescence microscopy.

## 2. Results and Discussion

### 2.1. Thermal Curing of Two-Part Epoxy Healing Chemistry

We first investigate the bulk curing kinetics of an epoxy system that has been previously used in microvascular-based, self-healing materials.<sup>[7]</sup> This system is composed of a 2.29:1 ratio of diglycidyl ether of bisphenol-A resin (EPON 8132) and an aliphatic amidoamine (Epikure 3046), both of which are commercially formulated with diluents to reduce their viscosity. To determine the effect of temperature on the healing reaction kinetics, studies are carried out at 30, 50, and 70 °C. Temperatures above 70 °C are not explored, as they lead to substantial weakening of the substrate material (see Supporting Information Figure S1).

The initial conversion of liquid monomer to polymer is probed using differential scanning calorimetry under isothermal conditions. The conversion fraction of reactive groups,  $\alpha$ , is obtained via measuring the cumulative heat evolved as a fraction of the heat of full reaction (490.5 J g<sup>-1</sup> with 10 °C min<sup>-1</sup> ramp). The empirical data show the initial conversion rate,  $d\alpha/dt = 7.1 \times 10^{-6}$  s<sup>-1</sup>, at 70 °C is two orders of magnitude greater than at 30 °C, such that nearly three times the monomer (74%) is reacted at 70 °C relative to 30 °C (27%) after 6 h (see Figure 2). Epoxy-amine reaction kinetics are often successfully described by the Kamal model,<sup>[14,16,17]</sup> which is an autocatalytic phenomenological model given by:

$$\frac{d\alpha}{dt} = (k_1 + k_2\alpha^m)(1 - \alpha)^n \quad (1)$$

where  $k_1$  and  $k_2$  are rate constants with Arrhenius temperature dependencies, and  $m$  and  $n$  are temperature-independent constants. By iteratively solving for these parameters,<sup>[18]</sup> this model successfully describes the data and is generalized to predict conversion for arbitrary temperatures (see Supporting Information Table S1).

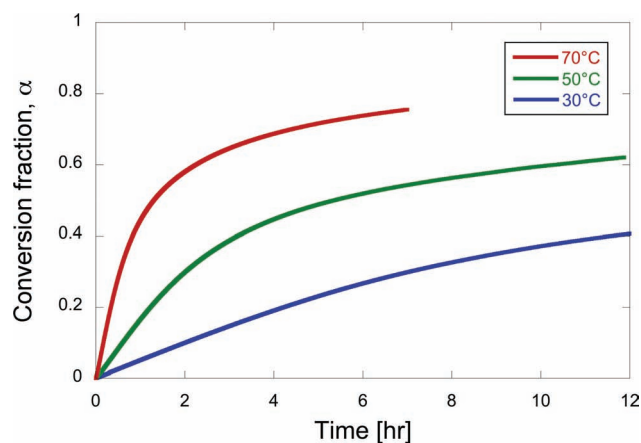


**Figure 2.** Epoxy curing reaction as a function of temperature. Data for degree of conversion,  $\alpha$ , is collected under isothermal conditions for stoichiometric mixtures of epoxy resin and hardener.

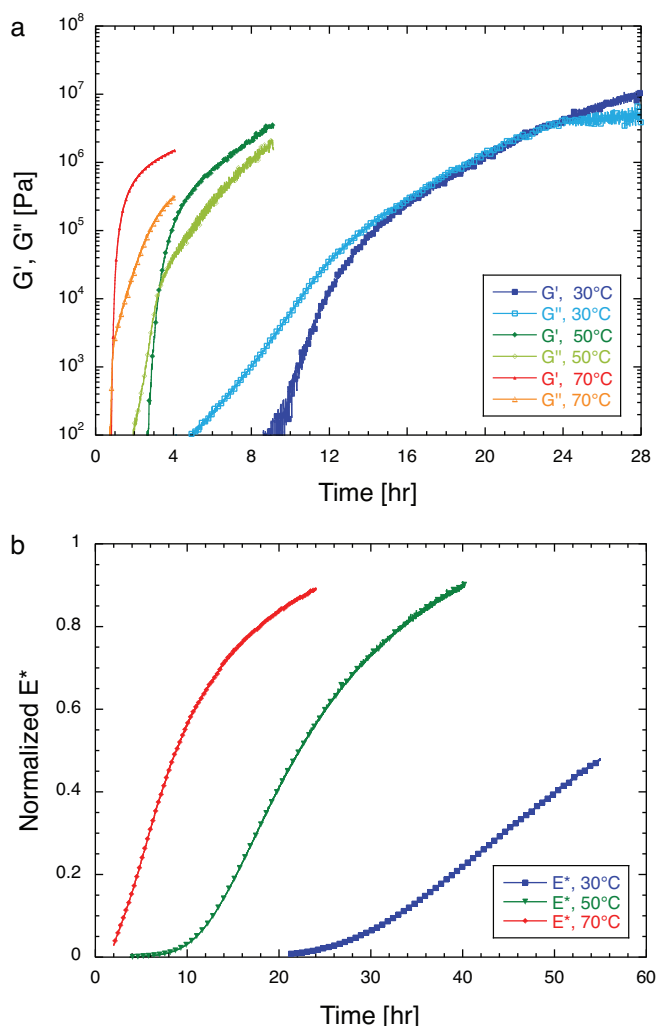


**Figure 3.** (a) Semilog plot of epoxy shear storage ( $G'$ ) and loss ( $G''$ ) moduli and (b) plot of complex modulus  $E^*$  normalized by the fully cured modulus for stoichiometric epoxy resin and hardener mixtures. The  $E^*$  data are measured at elevated temperatures and then scaled by ratios of  $E^*(50\text{ °C})/E^*(30\text{ °C})$  or  $E^*(70\text{ °C})/E^*(30\text{ °C})$  for a fully cured sample.

At intermediate times, we determine the effects of accelerated healing kinetics on epoxy gelation under isothermal conditions (Figure 3a). The gel point defines the transition from a predominantly viscous liquid to a spanning gel network, as denoted by the crossover in shear storage ( $G'$ ) and loss ( $G''$ ) moduli. At 30 °C, the epoxy gel point occurs at  $\sim 21$  h, after which polymerized material spans the width of the crack plane. By contrast, the gel point occurs at 3.1 h and 0.9 h for 50 and 70 °C, respectively. The twenty-fold reduction in the onset of gelation at 70 °C greatly shortens the residence time of the fully liquid regime within the crack plane. As a result, self-healing specimens would spend less time in a compromised mechanical state, during which any additional loading may exacerbate the damage incurred.

To probe the final stage of healing kinetics after gelation, flexure bars of the weakly elastic material are measured by dynamic mechanical analysis (DMA). At their respective temperatures, each bar is probed in a 3-point bend geometry

starting approximately 0.5 h after the onset of gel formation. For fully cured epoxy material, the complex modulus,  $E^*$ , is 1.06 GPa, 718 MPa, and 45.4 MPa at 30, 50, and 70 °C, respectively (see Supporting Information, Figure S2). Note, upon cooling the 50 °C and 70 °C samples to 30 °C, their complex moduli also exceed 1 GPa. To easily compare the complex moduli at elevated temperatures during polymerization, they are normalized by their fully cured moduli (Figure 3b). At 50 and 70 °C, the epoxy modulus begins to plateau near 90% of the fully cured modulus values at 40 h and 24 h, respectively. The 30 °C modulus reaches 40% of its fully cured value at  $\sim 50$  h, but the time required to reach this value is dramatically reduced to  $\sim 7$  h at 70 °C. From the perspective of repetitive healing, a specimen healed at 70 °C will complete at least seven cycles in the same time required to heal a specimen at 30 °C.

## 2.2. Direct-Write Assembly of Ternary Interpenetrating Microvascular Networks

To create self-healing materials capable of *in situ* thermal regulation, we designed an epoxy coating/substrate architecture with three interpenetrating microvascular networks (Figure 1a). Similar to the first self-healing system with dual interpenetrating microvascular networks,<sup>[1]</sup> two of these discrete networks are filled with an epoxy resin and amine hardener, respectively. In each case, vertical conduits are patterned that facilitate the transport of these healing agents from the underlying microvasculature to the brittle coating. The third microvascular network is designed to interdigitate between the vertical features, such that its circulation pathway is spatially localized near the damage region within the coating. Each network has a single input and output connected to a macroscale reservoir that supplies the healing or thermal fluids, respectively.

These ternary self-healing architectures are fabricated by direct-write assembly<sup>[19,20]</sup> of microcrystalline wax-based and aqueous Pluronic F127 fugitive inks, whose rheological behavior has been reported previously.<sup>[1]</sup> The desired microvascular networks are patterned by depositing wax ink filaments separated by Pluronic F127 ink filaments. Using this dual ink printing approach, an arbitrary number of isolated microvascular networks can be constructed. The microvascular networks that house the epoxy resin and hardener are composed of microchannels of 330  $\mu\text{m}$  in diameter, while the network that circulates fluid for thermal control consists of microchannels that are 200  $\mu\text{m}$  in diameter to facilitate their interdigitation between the printed vertical features. After the patterning is complete, the printed structure is first infiltrated with the substrate resin and cured and then the inks are sequentially removed. The Pluronic F127 ink is removed first and the resulting microchannels are infiltrated with substrate resin and cured. The microcrystalline wax is then removed to create three separate interpenetrating microvascular networks. For aid in visualization, these networks are infiltrated with different dyed fluids to demonstrate their isolated nature (Figure 1b). Finally, a brittle polymer coating, which is made opaque by the addition of carbon black, is applied to the specimen substrate. The coating opacity is designed to block background fluorescence from the underlying network during imaging of the healing fluids in the crack plane.

### 2.3. Thermal Regulation via Embedded Microvasculature

To demonstrate that this novel microvascular design provides sufficient thermal control in localized regions of damage, an epoxy/coating substrate architecture with an embedded ternary interpenetrating microvascular network is connected to a water circulation reservoir maintained at constant temperature ranging from 30–70 °C. The heated water is circulated within the third interdigitated network at a flow rate of 5 mL min<sup>-1</sup>.<sup>[4]</sup> The specimen is imaged with an infrared camera as a function of time to determine its surface temperature. Thermal images are acquired continuously at each temperature of interest (see movie, Supporting Information). The samples achieve thermal equilibrium in 5 min or less for each temperature explored, with values ~3–5 °C lower than the water reservoir. Sample images obtained after 10 min are shown in **Figure 4a–c**, in which the location of the circulating fluid microchannels are highlighted by the dashed white lines in **Figure 4a**. Water is used as the thermal fluid due to its high conductivity and heat capacity. However, this fluid may introduce small bubbles into the microvascular channels that divert flow and lead to minor variations in the temperature profiles. To obviate this, an alternate fluid, such as polyalphaolefin oil, could be used.<sup>[4]</sup>

### 2.4. Self-Healing of Ternary Interpenetrating Network Systems

To demonstrate the self-healing behavior of epoxy coating/substrate architectures with embedded ternary interpenetrating

microvascular networks, we tested them under 4-point bending using the test protocol reported previously.<sup>[6]</sup> The brittle coating is fractured at room temperature in a single location and fluorescently dyed epoxy resin and hardener wick into the crack plane. After healing for specified times while continuously circulating the heated fluid, samples are cooled to room temperature and mechanically tested to assess their healing efficiency. A heal stress,  $\sigma_{\text{heal}}$ , is calculated based on the healed peak load at fracture according to equation 2:

$$\sigma_{\text{heal}} = \frac{3 P_{\text{peak}} (L - L_i)}{2wt^2} \quad (2)$$

where  $P_{\text{peak}}$  is the peak load at fracture,  $L$  is the outer span length,  $L_i$  is the inner span length,  $w$  is the specimen width, and  $t$  is the specimen thickness. Average heal stresses are plotted as a function of time for the three temperature conditions explored (see **Figure 5**).

In these samples, healing is not observed prior to the onset of epoxy gelation. At 30 °C,  $t_{\text{gel}} \approx 21$  h and intermittent healing is observed after 24 h to 36 h. These samples required heal times of at least 42 h to achieve consistent mechanical restoration. By contrast,  $t_{\text{gel}} \approx 3.1$  and 0.9 h at 50 and 70 °C, respectively. At 50 °C, samples exhibit consistent healing after approximately 4 h, whereas only 1 h is required for samples held at 70 °C. Moreover, in each case, their average heal stress increases with time, since the epoxy curing reaction continues well beyond the gel point. To obtain the same degree of mechanical restoration,

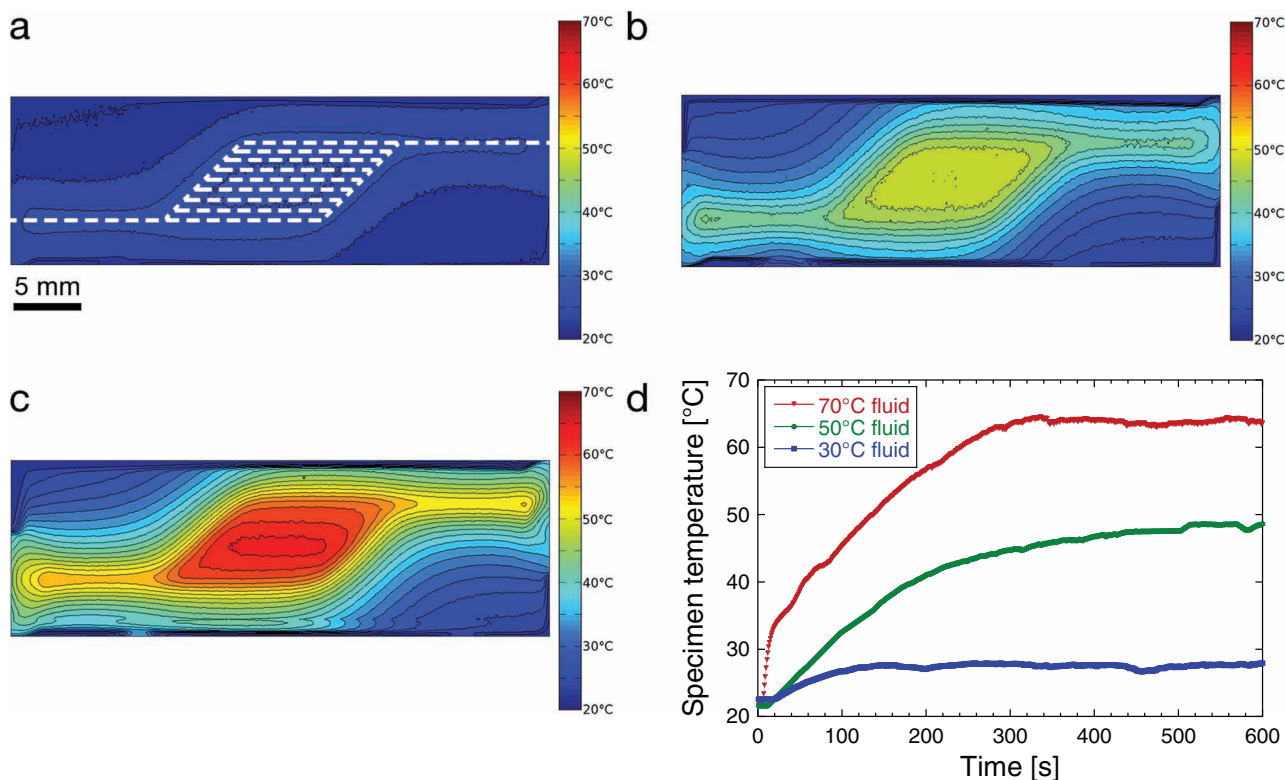


**Figure 4.** Infrared thermal imaging of epoxy coating/substrate architecture with embedded ternary microvascular networks acquired after circulating heated water for 10 minutes at a flow rate of 5 mL/min of varying temperature; (a) 30 °C, (b) 50 °C and (c) 70 °C. Contour lines denote temperature change of 2 °C. The location of the thermal regulating, microvascular network is indicated by dashed lines in (a), with flow direction from left to right. (d) Plot of the time-dependence of the average temperature of the region above the vertical conduits.

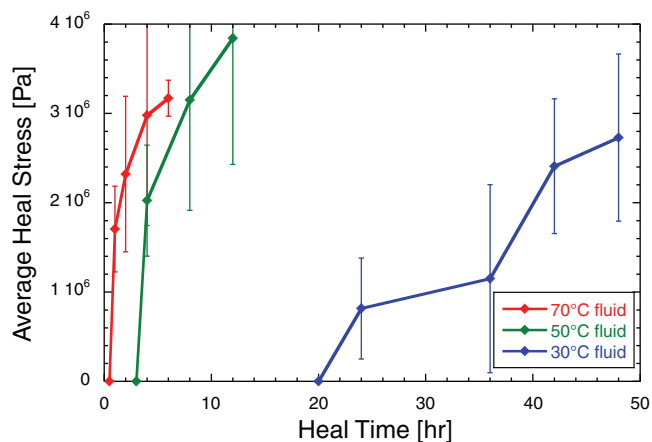


**Figure 5.** Average heal stress for epoxy coating/substrate architectures with embedded ternary interpenetrating microvasculature locally heated to 30, 50, or 70 °C as a function of heal time. Error bars denote one standard deviation for the samples tested. Fracture data is obtained after cooling to room temperature in all cases.

defined as the average original fracture stress (2.03 MPa), total healing times of 40, 4, and 1.5 h are required for samples held at 30, 50 and 70 °C, respectively. In addition to increased reliability at elevated temperatures, the concomitant decrease in healing times by an order of magnitude greatly accelerates mechanical recovery thereby reducing the downtime for damaged structures.

To investigate epoxy resin and hardener mixing in the crack plane upon fracture, the samples are imaged using fluorescence microscopy to determine the location of the dyed epoxy components. A representative image of the fracture region is shown in Figure 6a, where green and red fluorescence indicate the presence of epoxy resin and hardener, respectively. Clearly, a substantial fraction of the fluid is in either highly resin- or hardener-rich regions (Figure 6b). The average composition within the crack plane is 70% epoxy resin and 30% hardener, closely matching the 2-to-1 ratio of vertical conduits that deliver these healing agents to the crack plane. The composition distributions for comparable healing strengths are displayed in Figure 6c for healing times of 48, 8 and 4 h at 30, 50 and 70 °C, respectively. The distribution curves have strong peaks near both the pure hardener and pure resin compositions, which are irrespective of time or temperature (see Supporting Information, Figure S6). Two-part epoxy healing strongly depends upon the epoxy stoichiometry and mixing within the damaged region. Substantial polymerization only occurs for fully mixed compositions composed of 40–75 w/w% resin. As seen in Figure 6b–c, only ~20–30% of the crack plane volume contains compositions within this desired range. Prior self-healing studies based on single<sup>[6]</sup> and dual<sup>[7]</sup> microvascular network architectures have revealed similar incomplete curing, with only ~50% of the crack plane covered with polymerized epoxy material after multiple healing cycles.<sup>[7]</sup> Note, in poorly mixed regions, a weak gel with minimal elasticity likely forms, which is unable to contribute significantly to the overall recovery of mechanical strength.

To compare these observations to the predicted behavior, we estimate the characteristic timescales associated with epoxy

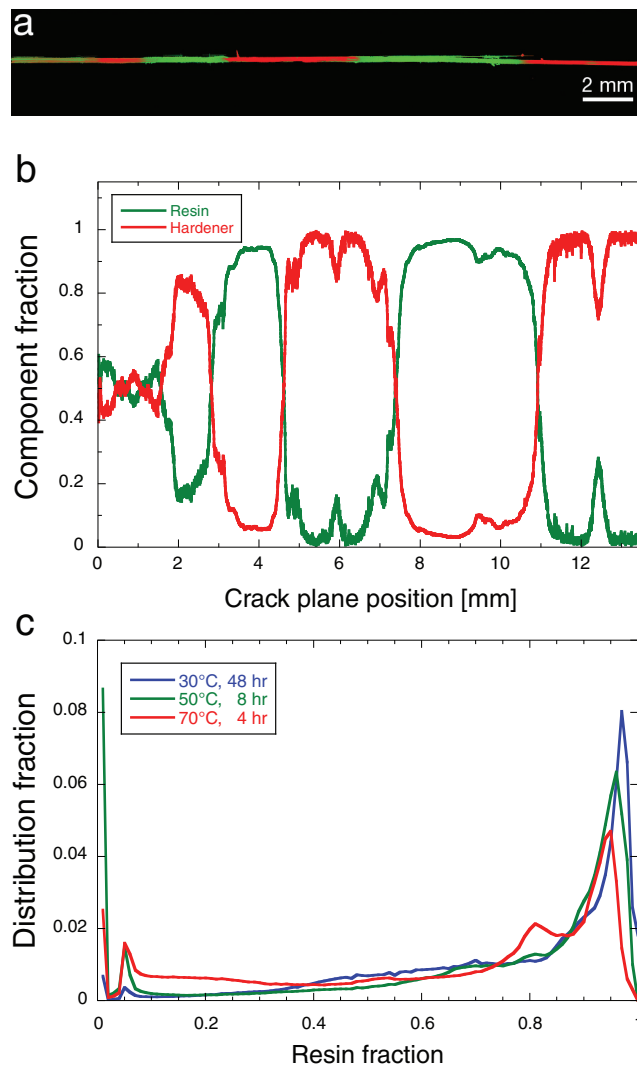


**Figure 6.** Epoxy mixing in the crack region. (a) Representative tiled image of fluorescently dyed epoxy resin (green) and hardener (red) that fill a crack region. (b) Resin and hardener composition fractions along the length of the crack. Compositions are sampled every 1.5 μm. (c) Composition distribution of epoxy resin and hardener that have partially mixed within the crack plane. Each line is the average for all specimens at the respective temperature.

flow within the crack plane,  $t_{flow}$ , diffusion,  $t_{diffusion}$ , and curing kinetics upon fracture  $t_{cure}$ . Immediately upon crack formation within the brittle coating, capillary forces induce fluid migration from the vertical conduits (330 μm in diameter) to the crack plane (width ≈ 50–100 μm). The pressure drop ( $\Delta P$ ) that drives fluid flow is given by Equation 3:

$$\Delta P = 2\gamma \cos \theta \left( \frac{1}{w} + \frac{1}{t} \right) - 2\gamma \cos \theta \left( \frac{1}{R} \right) \quad (3)$$

where  $\gamma$  is the liquid-vapor surface energy,  $\theta$  is the contact angle,  $w$  and  $t$  are the width and thickness of the coating crack opening, and  $R$  is the radius of the network channels (see Supporting Information, Figure S7).<sup>[21]</sup> This capillary driving

force is opposed by a viscous resistance to fluid flow,<sup>[22]</sup> as described by the Hagen-Poiseuille relationship for cylindrical channels:

$$\Delta P = \frac{32\mu LU}{D^2} \quad (4)$$

where  $\mu$  is the dynamic viscosity,  $L$  is the fluid path length within the microvascular network, and  $U$  is the linear velocity of the fluid within the network.<sup>[23]</sup> The minimum fluid velocity within the crack plane,  $U_{crack}$ , is determined for the longest path length,  $L$ , of  $\sim 28$  mm for both the epoxy resin ( $\gamma = 35.3$  mN m<sup>-1</sup>,  $\theta = 9^\circ$ ,  $\mu = 1.07$  Pa-s) and hardener ( $\gamma = 32.8$  mN m<sup>-1</sup>,  $\theta = 20^\circ$ ,  $\mu = 0.44$  Pa-s) by equating Equation. (3) and (4), and assuming conservation of fluid volume. For typical crack widths ranging from  $\sim 50$  to  $100$   $\mu$ m,  $t_{flow}$  ranges from 3.3 to 18.5 s for the resin and from 1.5 to 8.2 s for the hardener at room temperature. These estimated times are in good agreement with direct imaging of fluid flow, in which cracks fully filled within  $\sim 15$  s.

The epoxy resin and hardener will undergo diffusive mixing upon making contact within the crack plane.  $t_{diffusion}$  defines the time for a given fluid to diffuse across the characteristic length scale, i.e., half the distance between vertical conduits (500  $\mu$ m). The Einstein-Smoluchowski equation for molecular diffusion is given by:

$$t_{diffusion} = \frac{\langle x^2 \rangle}{2D} \quad (5)$$

where  $\langle x^2 \rangle$  is the root-mean square net displacement of the molecule. From Equation (5), we estimate  $t_{diffusion} \approx 6.5$  h for an initial  $D$  of  $5.2 \times 10^8$  cm<sup>2</sup>/s,<sup>[24]</sup> which is substantially longer than  $t_{flow}$ , but lower than  $t_{cure}$  (using the gelation time as a proxy). However, it is well known that the diffusivity decreases by a few orders of magnitude as the initial reaction proceeds to  $t_{cure}$ ,<sup>[25]</sup> which results in  $t_{diffusion} \gg t_{cure}$ . As shown in Figure S6, the extent of mixing does depend strongly on  $t_{cure}$ , because diffusion is greatly hindered within the crosslinked epoxy network. Mixing is also relatively independent of temperature increases, though the resin-rich peak broadens and shifts slightly to lower resin-to-hardener ratios (Figure 6c). Hence, the exponential increase in diffusivity with temperature is largely counterbalanced by an analogous increase in epoxy viscosity. Nevertheless, our observations reveal a slight difference between these two activation energies that weakly favors diffusive mixing at higher temperatures, and thus, further enhances healing.

### 3. Conclusions

We have constructed self-healing materials with embedded ternary interpenetrating microvascular networks by direct-write assembly of fugitive inks. Thermal characterization of the bulk two-part epoxy healing system revealed healing kinetics are accelerated by over an order of magnitude as the temperature increases from 30 to 70 °C. Localized heating in the damage regions is enabled by circulating a temperature-controlled fluid through the embedded microvasculature. Their mechanical behavior shows that the healing times are reduced by over an order of magnitude with increased dependability of restoration at elevated temperatures. This flexible design may find widespread use in large-scale

structural applications that would benefit from accelerated autonomic healing via localized, *in situ* thermal regulation.

### 4. Experimental Section

**Interpenetrating microvascular network fabrication:** Microcrystalline wax ink composed of 60 w/w% microcrystalline wax (SP-19, Strahl & Pitsch, Inc.) and 40 w/w% heavy mineral oil (Fischer Scientific) is prepared by stirring the molten components at 100 °C for 10 min. The heated solution is poured into 3 mL syringes (EFD, Inc.) and is rapidly quenched in an ice water bath to solidify the ink, after which the syringe is warmed to room temperature. The triblock-copolymer ink is prepared with 30 w/w% triblock copolymer (Pluronic F127, BASF) in deionized water. The copolymer is slowly added to an aqueous solution held at 5 °C. Upon full dissolution of the copolymer, the solution is refrigerated for >12 h to remove all air bubbles. The cooled solution is poured into 3 mL syringes and then warmed to ambient temperature.

Interpenetrating microvascular networks are deposited onto a cured epoxy substrate (Envirotext Lite, Environmental Technologies Inc.) via a three-axis motion-controlled robotic deposition stage (ABL9000, Aerotech Inc.). The fugitive wax and Pluronic F127 ink syringes are fitted with 200  $\mu$ m and 100  $\mu$ m nozzles (EFD Inc.), respectively, and mounted to the stage in air-pressure multiplier dispensers (HP7X, EFD Inc.) for extrusion at rates of 4 to 6 mm s<sup>-1</sup>. The fugitive ink networks are deposited in an alternating fashion, whereby each subsequent fugitive wax network is patterned onto the previously deposited Pluronic F127 support material. The order of wax network deposition is first the epoxy resin network (330  $\mu$ m feature diameter), followed by the epoxy curing agent network (330  $\mu$ m feature diameter), and ending with the thermal fluid circulation network (200  $\mu$ m feature diameter). The microchannel diameters are varied by dynamically controlling the applied extrusion pressure.<sup>[26]</sup> A detailed schematic fabrication flowchart is provided in the Supporting Information (Figure S3).

The patterned structures are infiltrated with Envirotext Lite epoxy matrix material and cured for 24 h at room temperature. Access to the Pluronic F127 networks is provided via diamond saw cuts to enable preferential dissolution of this fugitive ink in a water bath held at  $\sim 5$  °C for 12 h. The specimens are dried and the connected void volume is re-infiltrated with epoxy matrix material. Upon curing, the specimens are cut and polished to final dimensions (50 mm  $\times$  14 mm  $\times$  7 mm). The fugitive wax ink is melted at 85 °C for removal from the specimen via application of a light vacuum and any wax residue dissolved via ultrasonication with a 20 w/w% aqueous degreaser solution (VCPI-411, Cortec).

**Epoxy fluid measurements:** The epoxy resin and hardener viscosities are measured using a controlled-stress rheometer (C-VOR, Malvern Instruments, Malvern, UK) equipped with a cup and bob (C14, 14 mm bob diameter, 0.4 mm gap width) geometry at 25 °C. Contact angles for the components in contact with the brittle coating material are imaged with a digital camera (PowerShot S2 IS, Canon), with angles measured using ImageJ (NIH). Surface energies of the liquid-vapor interfaces of the healing components are measured with a tensiometer (250-CA, Ramé-Hart Instrument Co.) and are averaged over 30 sample measurements each.

**Differential Scanning Calorimetry (DSC):** Isothermal DSC tests are performed on a DSC (DSC821, Mettler-Toledo) at 30, 50 and 70 °C under a nitrogen atmosphere. The epoxy resin and hardener are stoichiometrically mixed in a 2.29:1 ratio of EPON 8132:Epikure 3046 within 60 s of test initiation. The measurement cell is pre-heated to minimize the transient heating time ( $<30$  s for 70 °C) to accurately capture initial reaction rates. Tests are stopped after 12 hr, when the reaction exotherm falls below the detection limits of the machine.

**Rheological measurements:** The shear storage and loss moduli,  $G'$  and  $G''$  respectively, of the epoxy system are measured with a controlled-strain rheometer (AR-G2, TA Instruments) using a parallel plate geometry (25 mm diameter). Stoichiometric mixtures of EPON 8132 and Epikure 3046 are placed in the geometry and isothermally held at 30, 50 or 70 °C.

Oscillatory measurements are performed at 1 Hz with 0.1% strain with a plate gap of ~600–800  $\mu\text{m}$ .

**Dynamic Mechanical Analysis (DMA):** The tensile storage and loss moduli,  $E'$  and  $E''$  respectively, of polymerizing epoxy material are determined by dynamic mechanical analysis (RSA III, TA Instruments). Stoichiometric EPON 8132 and Epikure 3046 mixtures are cured in an oven at 30, 50 or 70 °C until 30 min after the relevant gel point ( $G'/G''$  crossover). The bars (dimensions ~45 mm  $\times$  12 mm  $\times$  2 mm thick) are placed on the DMA in a 3-point bend geometry with a 25 mm span. The bend specimens are isothermally held at their respective temperatures and probed at 1 Hz at 0.2% strain.

**Thermal imaging:** The thermal surface profiles of specimens heated with circulating fluid are imaged with an infrared camera (DeltaTherm 1560, StressPhotonics Inc.). The specimen surface is painted black matte (Ultra-flat black, Krylon) for optimal imaging. A constant-temperature circulating bath (RTE-110, Neslab Instruments) with water is heated to 30, 50 or 70 °C and connected to a peristaltic pump (Model 7523-00, Cole-Parmer) set to an average flow rate of 5 mL  $\text{min}^{-1}$ . Fluid flow is commenced ~15 s following the start of image recording, with thermal profiles imaged at an interval of 1 s for 15 min in order to reach thermal equilibrium.

**Coating application:** The microvascular networks are infiltrated with a low-melting temperature wax (Purester 24, Strahl & Pitsch) to prevent the coating material from infiltrating the microchannels. The coating is composed of EPON 828 (Miller Stephenson Inc.), diethylenetriamine (Air Products Inc.), and Epikure 3253 (Miller Stephenson Inc.) mixed in a 100:15:7.5 weight ratio with a 0.2 w/w% addition of carbon black (Alfa-Aesar, Inc.) to mask the underlying microvasculature during fluorescence imaging studies. The epoxy coating is applied to the specimen surface and is cured at room temperature for 20 h. The coating is then polished to a final thickness of  $680 \pm 30 \mu\text{m}$ . The fugitive wax is removed by heating the specimen to 40 °C and flushing the specimen with petroleum ether (Fisher Scientific) three times, followed by flushing with xylenes (Acros Organics) three times.

**Mechanical fracture tests:** The two healing networks are filled with either epoxy resin (EPON 8132, Miller-Stephenson) or epoxy curing agent (Epikure 3046, Miller-Stephenson) that are fluorescently labeled with a rhodamine-based (DFSB-K87, Risk Reactor) or fluorescein-based dye (DFSB-K43, Risk Reactor), respectively. The coating is notched directly above vertical channel features using a test panel scratcher (Corrocutter 639, Erichsen) with a razor blade scribe under a constant load (6–10 N). The specimen is loaded in four-point bending and load-displacement data are recorded using LabVIEW (v.8.6, National Instruments).<sup>[6]</sup> Crack events are detected by an acoustic-emission sensor (model SE2MEG-P, Dunegan Engineering Company) and data collected with a digital oscilloscope (model LC584A, LeCroy). Load-displacement data are correlated with the acoustic emission data to determine the peak load at fracture. The specimen undergoes 50 flexural cycles at  $50 \mu\text{m s}^{-1}$  with an amplitude of 50  $\mu\text{m}$  to promote mixing.<sup>[1]</sup> Specimens are subsequently attached via tubing to a constant-temperature circulating bath (RTE-110, Neslab Instruments) and centrifugal pump (67705K36, McMaster-Carr) to circulate fluid at temperatures of 30, 50 or 70 °C. Specimens are returned to room temperature prior to testing of the healed coating. 8 specimens are averaged per final data point at each temperature and 5 specimens each all other data points.

**Fluorescence imaging and analysis:** Directly following heating, specimens are fluorescently imaged on an inverted microscope (DMI 6000B, Leica Microsystems) with a mercury-lamp source. Images are captured over the length of the crack plane using red ( $\lambda = 595 \text{ nm}$ ) and green ( $\lambda = 520 \text{ nm}$ ) filters under a 5X objective (see Supporting Information for experimental details). The grayscale filtered images are merged into one color image, and the color channels are resampled according to a composition calibration curve so that the photo color change linearly corresponds to a compositional change (see Supporting Information). Composition distribution curves are restricted to crack regions (ImageJ, NIH) and computed with MATLAB (v.2009b, MathWorks, Inc.) by dividing pixel ( $1.5 \mu\text{m} \times 1.5 \mu\text{m}$ ) composition data into bins of width equal to 1% compositional change.

## Supporting Information

Supporting Information is available from the Wiley Online Library or from the author.

## Acknowledgements

This work has been funded in part by the Air Force Office of Scientific Research Multidisciplinary University Research Initiative (Grant # F49550-05-1-0346). C. Hansen is supported by an NSF Graduate Student Fellowship and Dow Chemical through Grant #C7391. We thank Dr. Gavin Horn at the Advanced Materials Testing and Evaluation Laboratory and Brian Kozola for assistance with infrared thermal imaging, and John Vericella for help with tensiometry.

Received: July 9, 2011

Published online: September 14, 2011

- [1] C. J. Hansen, W. Wu, K. S. Toohey, N. R. Sottos, S. R. White, J. A. Lewis, *Adv. Mater.* **2009**, *21*, 4143.
- [2] S. R. White, N. R. Sottos, P. H. Geubelle, J. S. Moore, M. R. Kessler, S. R. Sriram, E. N. Brown, S. Viswanathan, *Nature* **2001**, *409*, 794.
- [3] R. B. Oueslati, D. Therriault, S. Martel, *IEEE Trans. Compon., Packag., Manuf. Technol.* **2008**, *31*, 869.
- [4] B. D. Kozola, L. A. Shipton, V. K. Natrajan, K. T. Christensen, S. R. White, *J. Intell. Mater. Syst. Struct.* **2010**, *21*, 1147.
- [5] N. W. Choi, M. Cabodi, B. Held, J. P. Gleghorn, L. J. Bonassar, A. D. Stroock, *Nat. Mater.* **2007**, *6*, 908.
- [6] K. S. Toohey, N. R. Sottos, J. A. Lewis, J. S. Moore, S. R. White, *Nat. Mater.* **2007**, *6*, 581.
- [7] K. S. Toohey, C. J. Hansen, J. A. Lewis, S. R. White, N. R. Sottos, *Adv. Funct. Mater.* **2009**, *19*, 1399.
- [8] E. N. Brown, N. R. Sottos, S. R. White, *Exp. Mech.* **2002**, *42*, 372.
- [9] J. D. Rule, E. N. Brown, N. R. Sottos, S. R. White, J. S. Moore, *Adv. Mater.* **2005**, *17*, 205.
- [10] M. M. Caruso, D. A. Delafuente, V. Ho, N. R. Sottos, J. S. Moore, S. R. White, *Macromolecules* **2007**, *40*, 8830.
- [11] A. R. Hamilton, N. R. Sottos, S. R. White, *Adv. Mater.* **2010**, *22*, 5159.
- [12] H. R. Williams, R. S. Trask, I. P. Bond, *Smart Mater. Struct.* **2007**, *16*, 1198.
- [13] H. R. Williams, R. S. Trask, I. P. Bond, *Compos. Sci. Technology* **2008**, *68*, 3171.
- [14] A. Yousefi, P. G. Lafleur, R. Gauvin, *Polymer Composites* **1997**, *18*, 157.
- [15] E. L. Kirkby, J. D. Rule, V. J. Michaud, N. R. Sottos, S. R. White, J.-A. E. Manson, *Adv. Funct. Mater.* **2008**, *18*, 2253.
- [16] M. R. Kamal, S. Sourour, *Polym. Eng. Sci.* **1973**, *13*, 59.
- [17] M. R. Kamal, *Polym. Eng. Sci.* **1974**, *14*, 231.
- [18] J. M. Kenny, *J. Appl. Polym. Sci.* **1994**, *51*, 761.
- [19] D. Therriault, S. R. White, J. A. Lewis, *Nat. Mater.* **2003**, *2*, 265.
- [20] D. Therriault, R. F. Shepherd, S. R. White, J. A. Lewis, *Adv. Mater.* **2005**, *17*, 395.
- [21] E. Delamar, A. Bernard, H. Schmid, A. Bietsch, B. Michel, H. Biebuyck, *J. Am. Chem. Soc.* **1998**, *120*, 500.
- [22] M. J. Cima, J. A. Lewis, A. D. Devoe, *J. Am. Chem. Soc.* **1989**, *72*, 1192.
- [23] F. M. White, in *Viscous Fluid Flow*, 3rd Ed., McGraw Hill, New York, USA **2006**, Ch. 3.
- [24] D. W. Larsen, J. H. Strange, *J. Polym. Sci.* **1973**, *11*, 65.
- [25] Y. Deng, G. C. Martin, *Macromolecules* **1994**, *27*, 5147.
- [26] W. Wu, C. J. Hansen, A. M. Aragon, P. H. Geubelle, S. R. White, J. A. Lewis, *Soft Matter* **2010**, *6*, 739.